# On the Polarimetric Variable Improvement via Alignment of Subarray Channels in PPAR Using Weather Returns

Igor R. Ivić

***Abstract*— Many modern phased-array radars (PARs) are multichannel systems that include multiple receivers for data acquisition. Each channel provides a signal from a group of Transmit/Receive modules comprising a section of the antenna. Channels typically consist of a full receive path, often with an independent local oscillator (LO) clock source. Such arrangement provides for beamforming flexibility on receive which can be applied in a digital domain. Consequently, the channel-to-channel phase and magnitude alignment is critical to maximizing the performance of the digital beamforming process and the accuracy of resulting detections and measurements. Herein, a novel method to improve such alignment using weather returns and achieve the improvement in the polarimetric variable estimates is described.**

***Index Terms*— Phased array radar (PAR), PAR calibration, radar polarimetry, radar signal processing, weather radar.**

## I. Introduction

THE phased-array radar (PAR) technology has been principally developed to advance point target detection and tracking, but recent efforts have been aimed at adopting this technology for weather observations [1]–[7]. Compared to weather observations with mechanically steered parabolic antennas, the PAR technology supports electronic beamsteering that enables more flexible scanning strategies [2], [4] and is shown to result in reduced data update times. Furthermore, one of the key advancements in weather radar technology is the polarimetric capability [8]. It entails transmission and reception of horizontally (H; polarization is in the horizontal plane) and vertically (V; polarization is in the vertical plane) polarized electromagnetic fields. Dual polarization provides new information that improves the effectiveness of forecasters and algorithms to distinguish between different types of precipitation (e.g., rain and hail) and nonweather scatterers (e.g., insects and ground clutter) [8]–[10]. Consequently, the future PAR systems will need to integrate the dual-polarization technology into a polarimetric PAR (PPAR) if intended for weather surveillance.

The set of estimates that polarimetric weather radars produce is Doppler spectral moments (i.e, reflectivity, velocity, and spectrum width [9], [10]) and polarimetric variables (differential reflectivity, copolar correlation coefficient, and specific differential phase [9], [10]). For the PPAR, polarimetric measurements drive the system requirements related to accuracy. The definitions of these measurements are as follows. The differential reflectivity ($Z_{\mathrm{DR}}$) is defined as the logarithm of the horizontal (H) to vertical (V) powers ratio of received signals. The copolar correlation coefficient [$\rho_{\mathrm{hv}}(0)$] is defined as the correlation coefficient between H and V returns, and the specific differential phase ($K_{\mathrm{DP}}$) is defined as the derivative of the differential phase (i.e., the argument of $\rho_{\mathrm{hv}}(0)$ denoted as $\phi_{\mathrm{DP}}$) with respect to range. Clearly, $\phi_{\mathrm{DP}}$ is the phase difference between the returns in H and V [9] at a given scanning direction and range. The main premise of the radar polarimetry is that the H and V two-way antenna patterns are well matched so that the main beam illuminates and receives echoes from the same scatterers in both polarizations.

Because weather surveillance radars (WSRs) are used to conduct quantitative measurements of weather phenomena (e.g., rain rate estimation), these systems require precise calibration [11], [12]. Consequently, one of the major obstacles to the use of PPAR technology for weather surveillance is the calibration needed to achieve measurements comparable to those of the systems using parabolic-reflector antennas [5]. This is due to the existence of significant cross-polar antenna patterns and the scan-dependent measurement biases caused by the variable antenna patterns with electronic beamsteering [13], [14]. The former induces cross coupling between returns from the horizontally and vertically oriented fields causing biases of polarimetric variable estimates. Furthermore, coupling in hardware is likely to exacerbate the cross-coupling effects. To mitigate these effects, a pulse-to-pulse phase coding in either the H or V ports of the transmission elements has been proposed [15]–[17]. This approach, however, does not address the scan-dependent measurement biases caused by the H and V copolar antenna patterns, which vary with beamsteering directions. The effects of these variations must be addressed via corrections using appropriate values at each boresight direction. If the cross-coupling effects are sufficiently suppressed with pulse-to-pulse phase coding and given

Manuscript received March 4, 2020; revised May 10, 2020; accepted June 14, 2020. Date of publication July 10, 2020; date of current version February 25, 2021. Funding was provided by NOAA/Office of Oceanic and Atmospheric Research under NOAA-University of Oklahoma Cooperative Agreement #NA16OAR4320115, U.S. Department of Commerce.

The author is with the Cooperative Institute for Mesoscale Meteorological Studies, The University of Oklahoma, Norman, OK 73072 USA, and is affiliated with the NOAA/OAR/National Severe Storms Laboratory, Norman, OK 73072 USA (e-mail: igor.ivic@noaa.gov).

Color versions of one or more of the figures in this article are available online at https://ieeexplore.ieee.org.

Digital Object Identifier 10.1109/TGRS.2020.3003293

a sufficiently narrow antenna main beam, the corrections can be conducted using only the knowledge of the copolar patterns [13]. Further, note that the efficacy of cross-coupling mitigation from pulse-to-pulse phase coding declines as the cross-polar pattern levels increase. Because this effect occurs inherently in PPARs as beams are electronically steered away from principal planes, there inevitably exist boresight directions for which cross-coupling mitigation is insufficient [13]. As a result, the correction using the measurement values of both the copolar and cross-polar patterns needs to be conducted at boresight directions where the cross-polar pattern levels are too high [13]. For example, the ratio of cross-polar to copolar pattern squared magnitudes must be less than approximately $-26$ dB, for patterns given in [13], to keep the worst case $Z_{DR}$ bias within $\pm 0.1$ dB when using pulse-to-pulse phase coding. Furthermore, the effects of active electronic components in transmit and receive paths in PAR systems can result in significant differences between transmit and receive patterns. For these reasons, it is important to characterize both transmit and receive copolar and cross-polar antenna patterns [18], [19].

Another aspect is that the majority of modern PAR systems utilize the subarray architecture on receive [20]. Hence, the multichannel PAR systems require phase coherency and magnitude alignment among receive subarray channels. For weather observations, such alignment is crucial because it affects the matching of receive H and V beam shapes and ultimately affects the quality of polarimetric measurements [21]. However, due to the hardware imperfections, the time series produced by the analog-to-digital converters (ADCs) in each channel intrinsically differ in magnitude and phase with respect to each other. Therefore, they must be aligned before summation to maximize the quality of the resulting two-way antenna patterns [22], [23]. Furthermore, in a typical system, drifts caused by temperature changes and thermal expansion affect the stability of subarray magnitudes and phases. Thus, a calibration process must be executed with a frequency sufficient to compensate for the drift in order to sustain the channel-to-channel coherency. For instance, such calibration may be achieved using a horn antenna placed in the phased-array antenna far field. With such an arrangement, channel-to-channel magnitude and phase differences can be measured using the test signal transmitted by the horn antenna and received by the PAR. Also, a test signal can be injected at an appropriate receiver point (e.g., at the downconverter input) in each channel to measure the phase differences induced by the path traversed by the test signal (but not accounting for the phase differences introduced by the hardware prior to the test signal injection). The described calibrations affect the quality of beams on receive but not on transmit (i.e., beams on transmit are not formed via subarray architecture and are typically less sensitive to drifts in system hardware). Hence, as receive patterns are improved, the two-way patterns are also improved because these are the products of transmit and receive beams.

Herein, an approach to estimate the subarray phase and magnitude differences using returns from weather scatterers of opportunity is presented. Such estimates are used to improve

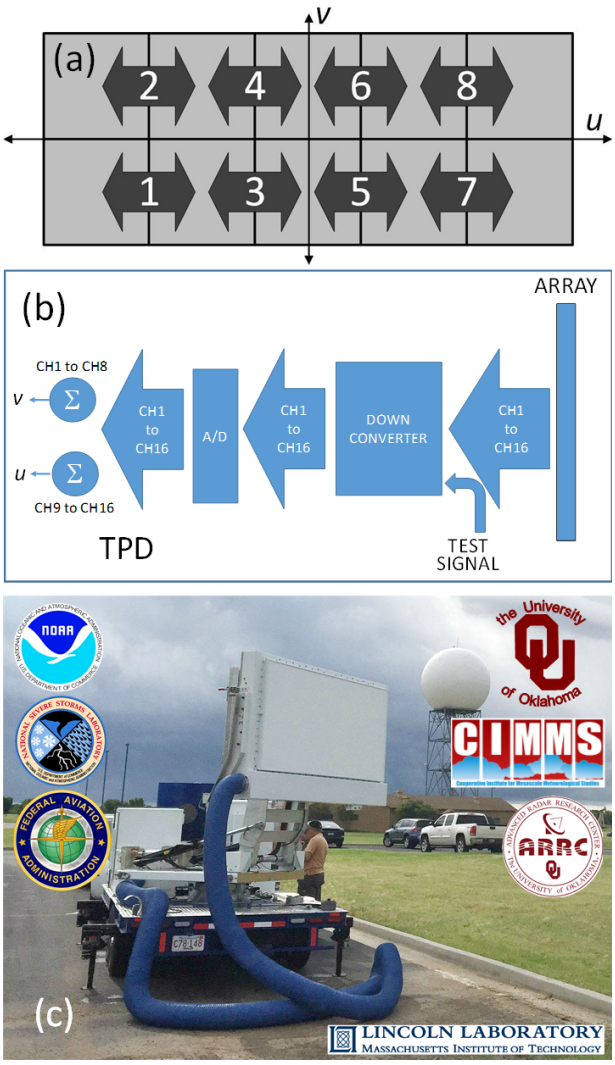


Fig. 1. (a) Antenna panel layout. On transmit, all panels act as a single antenna. On receive, the signals from adjacent panels are combined through an analog beamformer, creating an overlapped two-panel subarray structure. Blue arrows and numbers denote which panels form each of eight subarrays and subarray numbers. (b) TPD mobile system block diagram. (c) Photograph of TPD during data collection.

the alignment of the time series produced by individual subarrays. This article is structured as follows. The system setup is described in Section II. Analytical analysis is presented in Section III to provide a theoretical background for the measurement approach. Note that the framework for this analysis relies on previous works as indicated in the text. Experimental evaluation is presented in Section IV. The main conclusions of this article are summarized in Section V.

## II. System Setup

In this section, a system setup used to evaluate the method for channel-to-channel phase and magnitude measurements is described. It is based on a mobile planar PPAR, which is the product of multiagency collaboration [Fig. 1(c)]. The radar has been built by MIT Lincoln Laboratory in cooperation with the Advanced Radar Research Center (ARRC). It is operated by the National Severe Storms Laboratory (NSSL) and Cooperative Institute for Mesoscale Meteorological

Studies (CIMMS) [24], [25]. The radar antenna contains ten panels arranged in 2 × 5 matrix. Each panel consists of 8 × 8 matrix of radiating elements separated by a half-wavelength. Such an arrangement results in a 7° × 3° beamwidth at broadside. On receive, the antenna design is based on the overlapped subarray approach, which produces low sidelobes that suppress grating lobes outside of the main beam of the subarray pattern [20]. Each of the eight subarrays consists of two panels [Fig. 1(a)] and the operating frequency band of the antenna is 2.7–2.9 GHz. The radar is used for evaluating the suitability of planar PPAR technology for weather applications as part of the effort led by the National Severe Storms Laboratory (NSSL). The radar is referred to as Ten Panel Demonstrator (TPD).

Associated with each TPD subarray is a full receive path that includes a downconverter and ADC [Fig. 1(b)]. Such design produces 16 time series (or IQ) streams. The main (or copolar) polarization of the IQ streams from the first eight channels is along $v$ principal axis [vertical if the antenna is in landscape position as in Fig. 1(c)] and along $u$ principal axis [horizontal if the antenna is in landscape position as in Fig. 1(c)] for the channels 9–16 [Fig. 1(a)]. The TPD has no real-time data-processing capability and all 16 IQ streams are recorded for offline processing. To obtain the time series from combined IQ streams for polarization along $v$, data from channels 1–8 are coherently summed to produce one set of time series. The same procedure is applied to channels 9–16 to produce IQ time series for $u$ polarization. Obviously, the data from the two sets of channels must be aligned in magnitude and phase to yield the best possible two-way antenna patterns in both polarizations.

To measure the phase fluctuations in each of 16 receivers, test signals are injected at the input of every downconverter [Fig. 1(b)]. Measurements of these test signals provide instant channel-to-channel phase differences that are incurred by the downconverters and the subsequent circuity. Such measurements, however, do not account for the phase differences induced by the hardware components before downconverters. Furthermore, the test signals are obscured by the transmitted leakage pulse (i.e., a portion of the transmit pulse that leaks into the receive channel) during normal operation which prevents the monitoring of phase drift in parallel with data collection. To circumvent this issue, data collection is intermittently interrupted [i.e., high-power amplifiers (HPAs) are briefly turned off] to perform the test signal measurements. This capability is built into the scan strategies so that no operator intervention is required and the impact on data collection is minimal. Consequently, the test signal measurement data are embedded with the rest of the time series and is retrieved during offline processing.

The test signal measurements can be used to assess the phase differences among channels and create the set of unit modulus complex numbers that are used to remove the channel-to-channel phase differences incurred by the downconverters and the subsequent hardware. These numbers are referred to as beamforming coefficients (BFCs). Then, each combined sample $V_c(k, m)$ ($c$ is 'h' or 'v' which denote H or V polarization and '$v$' or '$u$' to denote polarizations along $v$ or $u$ principal axis) from range location at distance $k\Delta r$ ($k$ is the sample number in the range and $\Delta r$ is the distance between adjacent samples) relative to the radar in H and V is produced as

$$V_c(k, m) = \sum_{i=0}^{N_s-1} \mathrm{BFC}_c(i) V_c(k, m, i) \tag{1}$$

where $N_s$ is the number of subarrays per polarization (e.g., 8 in the case of TPD), and $i$ denotes the subarray number. In (1), $i$ denotes the subarray receiver number, and $m$ is the pulse number in a dwell.

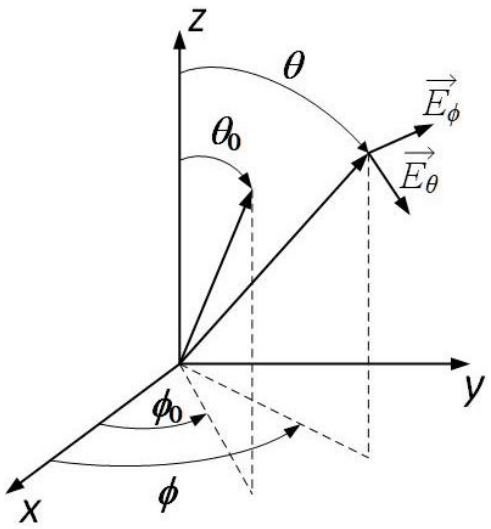


Fig. 2. Spherical coordinate system used to plot radiation patterns. It is assumed that the antenna face is aligned with the $yz$ plane.

## III. Theoretical Analysis

Herein, a theoretical model using a subvolume-based approach (presented in [16]) is assumed whereby weather signals received in H and V are viewed as the sum of incremental voltages caused by a large number of scatterers contained in subvolumes (bound by the specified resolution of antenna patterns in azimuth and elevation). The analysis is carried out assuming that the hydrometeors are oblate spheroids whose net mean canting angle is close to zero [26] so no depolarization on propagation and on scattering is present [26]–[28]. Note that in general, the canting angle (i.e., the angle between the incident vertically oriented electric field and the projection of the axis of symmetry on the plane of polarization) is not necessarily zero (e.g., due to wobbling). However, if the mean canting angle of scatterers in all subvolumes (i.e., net mean canting angle) comprising the region of interest is zero, then it may be assumed that the only depolarization is that induced by the system [26]. An assumption that the net mean canting angle is zero reflects properties of most hydrometeors encountered in observations (e.g., rain) but is not always true [29], [30]. It is also assumed that the difference in attenuation between H and V along the path of propagation can, for most observations at ∼10-cm wavelengths, be neglected, but the differential phase ($\phi_{\mathrm{DP}}$) [9], [27] cannot. As the beam is electronically steered at $\theta_0$, $\phi_0$ (where $90° - \theta_0$ is elevation and

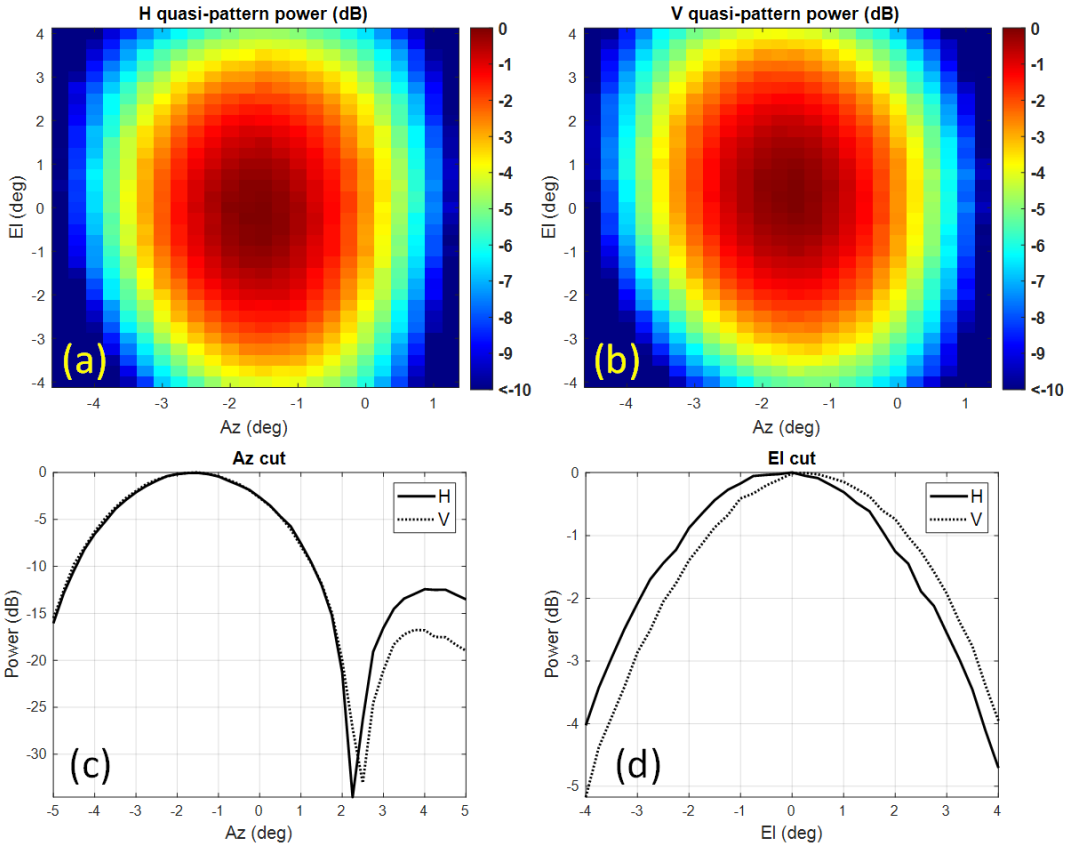


Fig. 3. 2-D receive copolar quasi-patterns for polarizations along (a) $u$ (or H) and (b) $v$ (or V) as well as (c) azimuth and (d) elevation cuts.

$\phi_0$ is azimuth) and $M$ pulses are transmitted simultaneously, in H and V, the total received voltages (from H and V in each $i$th subarray), at distance $k\Delta r$, are integrations over $\theta$ and $\phi$ (Fig. 2) as

$$\begin{aligned} V_{\rm h}(k,m,i) &= C_{\rm h}(i)\int_{\Omega}\left\{\begin{bmatrix} F_{\rm th}^{\rm co}SF_{\rm rh}^{\rm co}(i)s_{\rm hh}(k,m) \\ +F_{\rm th}^{\rm x}SF_{\rm rh}^{\rm x}(i)s_{\rm vv}(k,m)\end{bmatrix}e^{j\alpha_{\rm h}(m)}\right. \\ &\quad\left.+\begin{bmatrix} F_{\rm tv}^{\rm x}SF_{\rm rh}^{\rm co}(i)s_{\rm hh}(k,m) \\ +F_{\rm tv}^{\rm co}SF_{\rm rh}^{\rm x}(i)s_{\rm vv}(k,m)\end{bmatrix}e^{j\alpha_{\rm v}(m)}\right\}d\Omega+N_{\rm h}(i) \\ V_{\rm v}(k,m,i) &= C_{\rm v}(i)\int_{\Omega}\left\{\begin{bmatrix} F_{\rm tv}^{\rm x}SF_{\rm rv}^{\rm x}(i)s_{\rm hh}(k,m) \\ +F_{\rm tv}^{\rm co}SF_{\rm rv}^{\rm co}(i)s_{\rm vv}(k,m)\end{bmatrix}e^{j\alpha_{\rm v}(m)}\right. \\ &\quad\left.+\begin{bmatrix} F_{\rm th}^{\rm co}SF_{\rm rv}^{\rm x}(i)s_{\rm hh}(k,m) \\ +F_{\rm th}^{\rm x}SF_{\rm rv}^{\rm co}(i)s_{\rm vv}(k,m)\end{bmatrix}e^{j\alpha_{\rm h}(m)}\right\}d\Omega+N_{\rm v}(i). \end{aligned} \tag{2}$$

In (2), $d\Omega \equiv \sin(\theta)d\theta d\phi$ (integration along the range is omitted as it has no bearing on the results), while $N_{\rm h}(i)$ and $N_{\rm v}(i)$ are subarray noise powers in H and V. Further, symbols $C_{\rm h}(i)$ and $C_{\rm v}(i)$ stand for the complex numbers which describe the gain and phase imposed by the $i$th subarray H and V receive paths from the point of test signal injection to the A/D converters.

Symbols $F_{\rm th}^{\rm co}$ and $SF_{\rm rh}^{\rm co}(i)$ denote the copolar patterns (i.e., fields concomitant with $\vec{E}_{\phi}$ in Fig. 2) in H on transmit and receive, respectively. Note that the transmit patterns are the same for all subarrays as the subarray architecture pertains to receive only. For this reason, the letter "$S$" is included in the receive pattern notation. Symbols $F_{\rm th}^{\rm x}$ and $SF_{\rm rh}^{\rm x}(i)$ denote the same but for cross-polar patterns in H (i.e., fields concomitant with $\vec{E}_{\Theta}$ in Fig. 2). Analogously, $F_{\rm tv}^{\rm co}$, $SF_{\rm rv}^{\rm co}(i)$, $F_{\rm tv}^{\rm x}$, and $SF_{\rm rv}^{\rm x}(i)$ denote the same but for copolar (i.e., fields concomitant with $\vec{E}_{\Theta}$ in Fig. 2) and cross-polar (i.e., fields concomitant with $\vec{E}_{\phi}$ in Fig. 2) patterns in V. Note that each $F_{lp}^{q}$ (indices $l$ can be either "t" or "r," $p$ is either "h" or "v," and $q$ is either "co" or "x") is a one-way electric field pattern that is a complex function that depends on boresight direction $\theta_0$, $\phi_0$ (Fig. 2). In the described model, the transmit patterns characterize all active and passive components in the H and V transmit paths. The subarray receive patterns describe the system from the point where the antenna elements receive the incident radiation to the points of test signal injections. Symbols $s_{\rm hh}(k,m)$ and $s_{\rm vv}(k,m)$ denote the intrinsic echo voltages, from every subvolume, which would be received in H and V channels, respectively, if $F_{lp}^{\rm co}=1$ and $F_{lp}^{\rm x}=0$. Their properties are described by Doppler spectral moments (i.e., power in H and V, velocity, and spectrum width [9]) and polarimetric variables (i.e., differential reflectivity, copolar correlation coefficient, and differential phase [9]). They also contain the dependence on attenuation and differential phase with range (i.e., $\arg\{\langle s_{\rm hh}^{*}(k,m)\ s_{\rm vv}(k,m)\rangle\}=\phi_{\rm DP}$). In (2), $\alpha_{\rm h}(m)$ and $\alpha_{\rm v}(m)$ are optional pulse-to-pulse phase codes imposed on transmission in H and V channels, respectively. These may be applied to improve the cross-polar isolation during simultaneous transmit simultaneous receive (STSR)

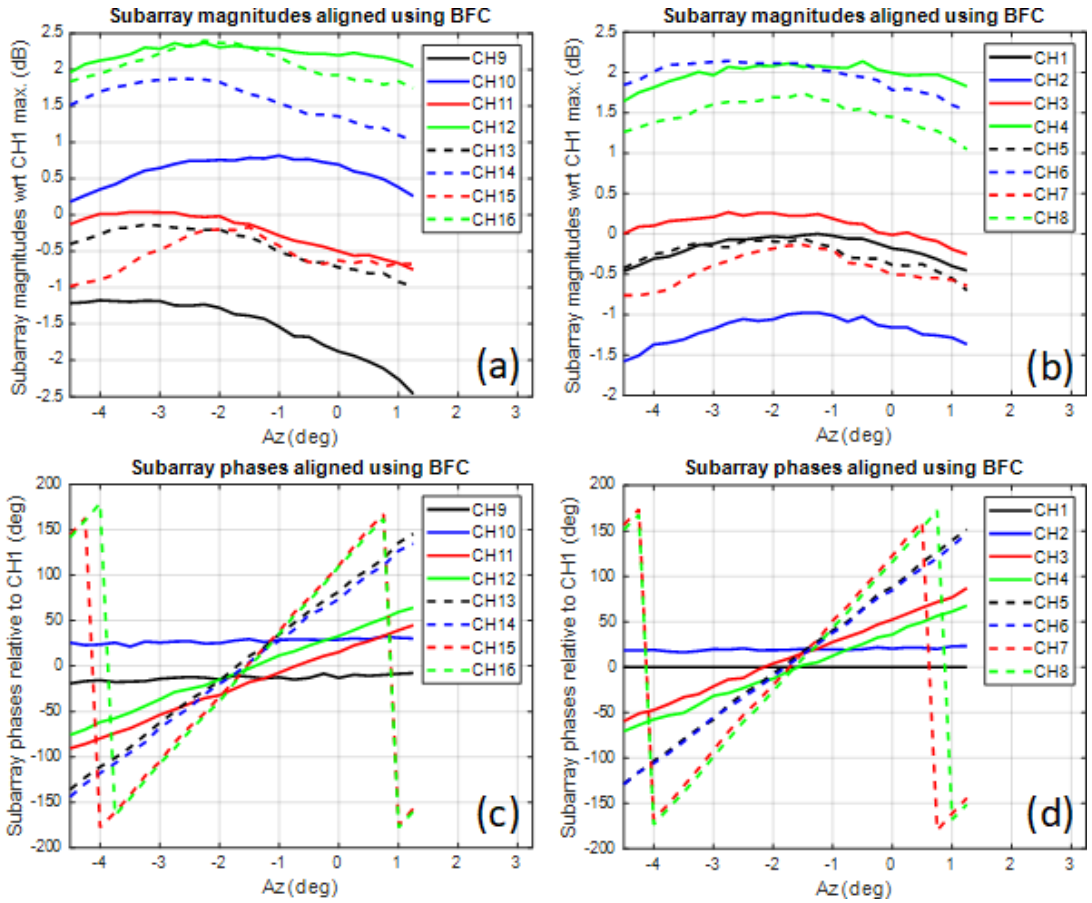


Fig. 4. Azimuth cuts (at elevation determined by the peak of the main beam formed from channels 1–8) for subarrays polarized along $u$ (or H), (a) magnitudes and (c) phases, and along $v$ (or V) (b) magnitudes and (d) phases. BFCs are produced using the test signal measurements.

mode via the phase coding method [15], [16] (i.e., PCSTSR mode).

The signal powers in each subarray and the cross-correlations between the subarray channels $i_0$ and $i_1$ in H, as well as V, are computed as

$$\hat{S}_{sc}(k,i_0) = \frac{1}{M}\sum_{m=0}^{M-1}|V_c(k,m,i_0)|^2 - N_c(i_0)$$
$$\hat{R}_{sc}(k,i_0,i_1) = \frac{1}{M}\sum_{m=0}^{M-1}V_c(k,m,i_0)V_c^*(k,m,i_1). \quad (3)$$

Assuming the main beams of two-way patterns of all subarrays encompass the same volume of space which is filled with weather scatterers (represented by Doppler spectral moments and polarimetric variables), the ensemble averages are

$$\begin{aligned}&\left\langle \hat{S}_{sc}(k,i_0)\right\rangle \\ &= |C_c(i_0)|^2\int_\Omega \left|F_{tc}^{co}SF_{rc}^{co}(i_0)\right|^2\left\langle|s_{cc}(k,m)|^2\right\rangle d\Omega \\ &\quad + \left\langle \Delta\hat{S}_{sc}(k,i_0)\right\rangle \\ &\left\langle \hat{R}_{sc}(k,i_0,i_1)\right\rangle \\ &= C_c(i_0)C_c^*(i_1)\int_\Omega \left|F_{tc}^{co}\right|^2 SF_{rc}^{co}(i_0)SF_{rc}^{co*}(i_1)\left\langle|s_{cc}(k,m)|^2\right\rangle d\Omega \\ &\quad + \left\langle \Delta\hat{R}_{sc}(k,i_0,i_1)\right\rangle. \quad (4)\end{aligned}$$

Note that the terms with symbol $\Delta$ stand for a linear combination of products among copolar and cross-polar patterns and cross-polar patterns only. Because the ensemble averages in (4) are dominated by the products that contain copolar patterns only, the terms with the symbol $\Delta$ can be considered as residuals. Nonetheless, these residuals induce cross-coupling effects that lead to biases in the estimates of polarimetric estimates [5]. The effect of these terms can be mitigated by using the pulse-to-pulse phase coding (i.e., PCSTSR mode) which is designed so that

$$\sum_{m=0}^{M-1} e^{j[\alpha_v(m)-\alpha_h(m)]} = 0. \quad (5)$$

Next, the correlation coefficient between subarrays $i_0$ and $i_1$ (i.e., the subarray correlation coefficient) in either H or V channel can be estimated by averaging in range as

$$\hat{\rho}_{sc}(i_0,i_1) = \frac{1}{K}\sum_{k=0}^{K-1}\frac{\hat{R}_{sc}(k,i_0,i_1)}{\sqrt{\hat{S}_{sc}(k,i_0)\hat{S}_{sc}(k,i_1)}} \quad (6)$$

where $K$ is the number of range locations at which time series are used for estimation. Further, if the effects of residuals in (4) are neglected and the radar beams are filled with weather scatterers of statistically isotropic properties (i.e., the terms $\langle|s_{cc}(k,m)|^2\rangle$ in (4) can be placed in front of the integral),

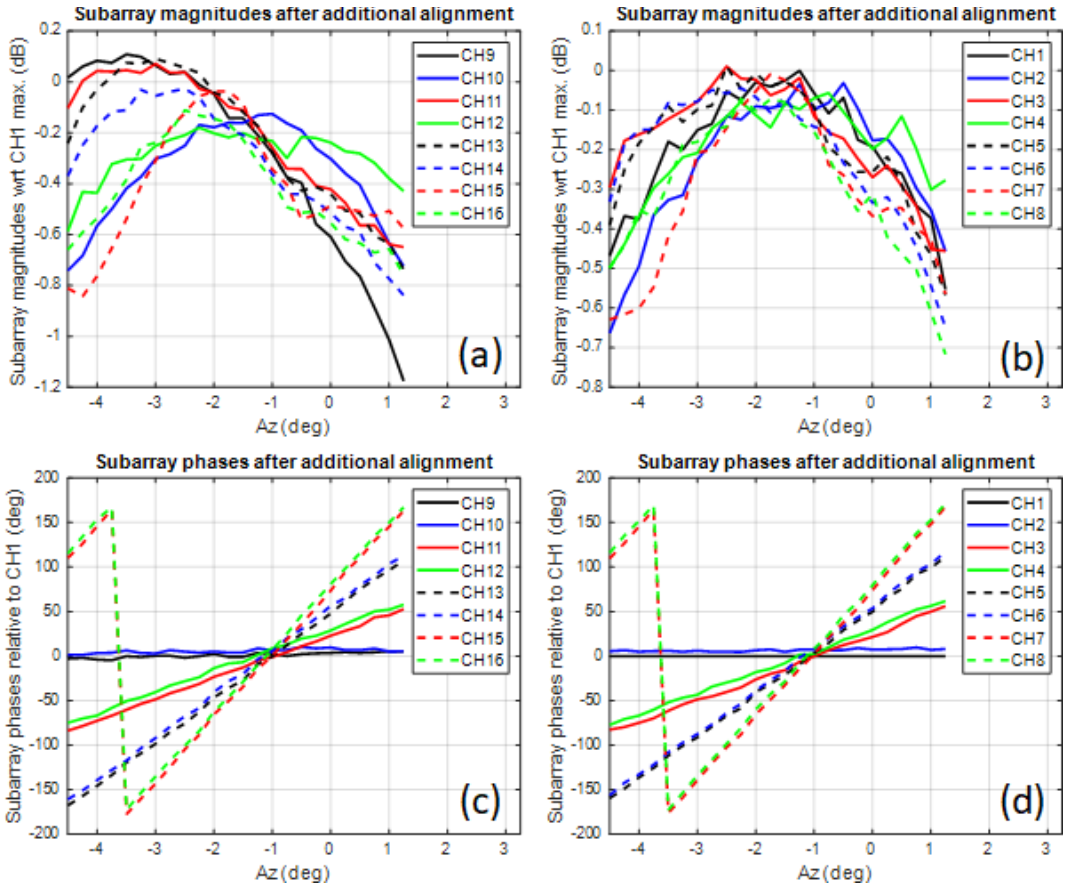


Fig. 5. Subarray magnitudes and phases for (a) and (c) H, and (b) and (d) V polarizations after additional alignment.

the ensemble average is

$$\begin{aligned}\langle \hat{\rho}_{sc}(i_0,i_1)\rangle &\approx \frac{1}{K}\sum_{k=0}^{K-1}\frac{\langle \hat{R}_{sc}(k,i_0,i_1)\rangle}{\sqrt{\langle \hat{S}_{sc}(k,i_0)\rangle\langle \hat{S}_{sc}(k,i_1)\rangle}}\\ &\approx \frac{C_c(i_0)C_c^*(i_1)}{|C_c(i_0)||C_c(i_1)|}\\ &\quad\times\frac{\int_\Omega \left|F_{tc}^{co}\right|^2 \mathrm{SF}_{rc}^{co}(i_0)\mathrm{SF}_{rc}^{co*}(i_1)d\Omega}{\sqrt{\int_\Omega \left|F_{tc}^{co}\mathrm{SF}_{rc}^{co}(i_0)\right|^2 d\Omega\times\int_\Omega \left|F_{tc}^{co}\mathrm{SF}_{rc}^{co}(i_1)\right|^2 d\Omega}}.\end{aligned}\quad(7)$$

The expression (7) indicates that the subarray correlation coefficient measured using distributed scatterers (e.g., weather) depends only on the system properties. Note that the mathematical expectation of the subarray correlation coefficient is a product of two terms whereby the first term describes the system effects from the test signal injection point down to A/D converters, while the second term describes the system up to that point. Furthermore, the modulus and the argument are

$$\begin{aligned}&\langle|\hat{\rho}_{sc}(i_0,i_1)|\rangle\\ &\quad\approx\frac{\left|\int_\Omega \left|F_{tc}^{co}\right|^2 SF_{rc}^{co}(i_0)SF_{rc}^{co*}(i_1)d\Omega\right|}{\sqrt{\int_\Omega \left|F_{tc}^{co}SF_{rc}^{co}(i_0)\right|^2 d\Omega\times\int_\Omega \left|F_{tc}^{co}SF_{rc}^{co}(i_1)\right|^2 d\Omega}}\\ &\langle\arg\{\hat{\rho}_{sc}(i_0,i_1)\}\rangle\\ &\quad\approx\arg\left\{C_c(i_0)C_c^*(i_1)\times\int_\Omega \left|F_{tc}^{co}\right|^2 SF_{rc}^{co}(i_0)SF_{rc}^{co*}(i_1)d\Omega\right\}\end{aligned}\quad(8)$$

which indicates that the argument of the subarray correlation coefficient can be used to estimate the system-imposed phase difference between subarrays $i_0$ and $i_1$.

The ratio of signal powers

$$\begin{aligned}\widehat{\mathrm{SR}}_c(i_0,i_1)&=\frac{1}{K}\sum_{k=0}^{K-1}\frac{\hat{S}_{sc}(k,i_0)}{\hat{S}_{sc}(k,i_1)}\\ \left\langle\widehat{\mathrm{SR}}_c(i_0,i_1)\right\rangle&\approx\frac{|C_c(i_0)|^2\int_\Omega\left|F_{tc}^{co}\mathrm{SF}_{rc}^{co}(i_0)\right|^2 d\Omega}{|C_c(i_1)|^2\int_\Omega\left|F_{tc}^{co}\mathrm{SF}_{rc}^{co}(i_1)\right|^2 d\Omega}\end{aligned}\quad(9)$$

can be used to estimate the system-imposed difference between subarray powers.

Given a reference subarray $i_{\mathrm{ref}}$, each existing $i$th subarray beamforming coefficient $[\mathrm{BFC}_c(i)]$ can be updated as

$$\widehat{\mathrm{BFC}}_c(i)=\mathrm{BFC}_c(i)\sqrt{\widehat{SR}_c(i_{\mathrm{ref}},i)}\exp(j\arg\{\hat{\rho}_{sc}(i_{\mathrm{ref}},i)\}).\quad(10)$$

In the system setup described herein, $\mathrm{BFC}_c(i)$ are obtained using test signals. If the system-based infrastructure for creating BFCs is not available, each $\mathrm{BFC}_c(i)$ may be set to one and weather returns can be used to compute estimates in (8) and (9). Then, BFCs may be updated as described in (10). This method is named the subarray alignment procedure (SAP).

## IV. Experimental Evaluation

The experimental evaluation is conducted on two types of data. The first type was collected in a clear air whereby the horn antenna was placed on top of a building located

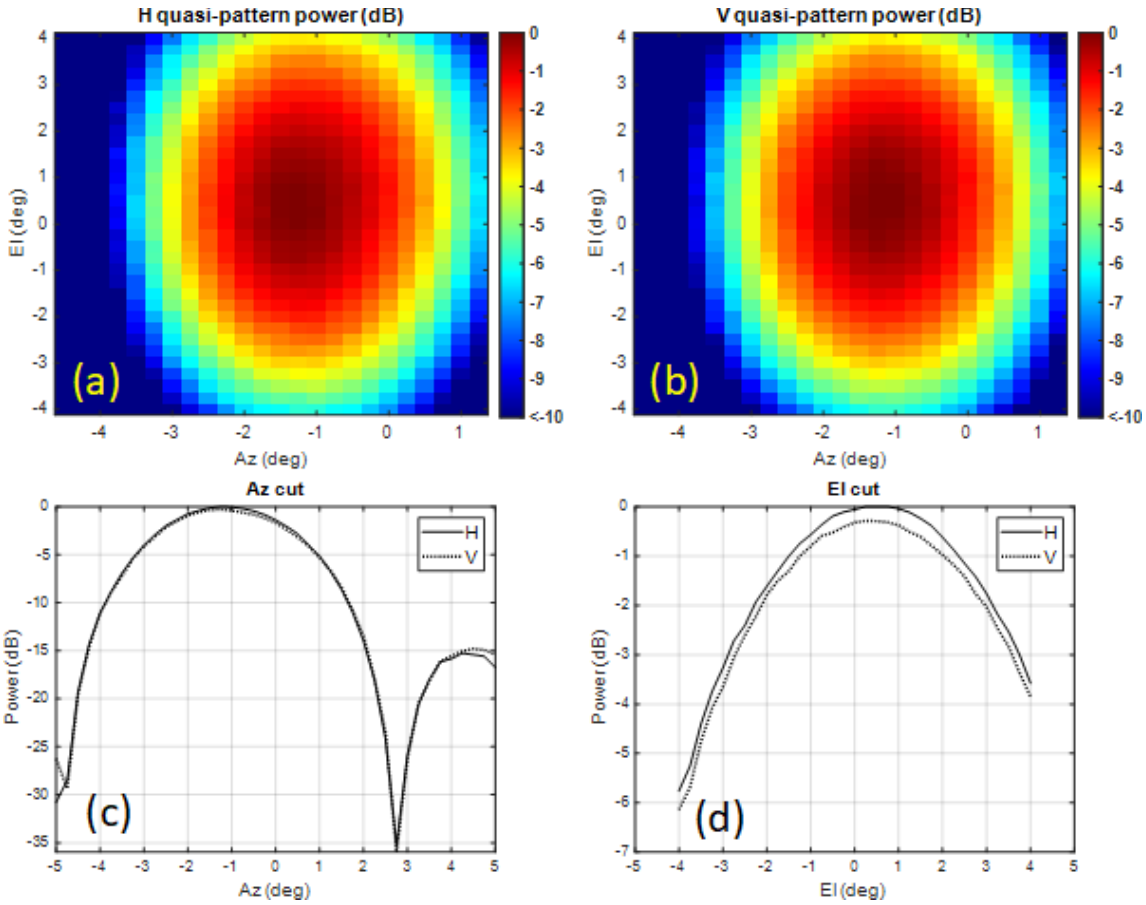


Fig. 6. 2-D receive copolar quasi-patterns for (a) H and (b) V as well as (c) azimuth and (d) elevation cuts after additional alignment.

∼1.6 km away from TPD. The horn antenna was placed in a 45° slanted position and used to illuminate TPD by connecting it to an RF generator. TPD data were collected in receive-only mode (HPAs were disabled) and by electronically steering the receive beam around the assumed horn antenna location. This produced two-dimensional pattern-like data for each subarray in H and V. It was found that these patterns can be used as a proxy for true antenna patterns and are herein referred to as quasi-patterns. These data are used to assess the quality of the array receive quasi-patterns and to demonstrate the importance of subarray phase and magnitude alignment. The collection of this type of data requires significant infrastructure and is, therefore, not conducive to regular collections. The second data type was collected in light-to-moderate rain while the radar antenna was at vertical incidence (i.e., the antenna was parallel to the ground and pointed toward the sky) and the beam was steered electronically to illuminate the scan area. These data are used for the experimental evaluation of the proposed SAP using weather returns (as it can be conducted whenever sufficient weather echoes are available). The results of these evaluations are described next.

### *A. Evaluation Using a Horn Antenna*

The results of the quasi-pattern measurement are shown in Fig. 3. The quasi-patterns are synthesized using the unit modulus BFCs with phases measured using the test signals. Visual comparison of Fig. 3(a) and (b) indicates a mismatch between H and V quasi-patterns. The differences are further demonstrated in Fig. 3(c) and (d) where cuts along azimuth and elevation are shown. Next, the effects of H and V copolar beam mismatches on the polarimetric variable estimates are considered.

The polarimetric variable estimates of interest at each range location $k$, in the STSR mode, are computed from the second-order estimates as in [31] [see eq, (12)]. The second-order estimates are $\hat{S}_{\rm h}$ and $\hat{S}_{\rm v}$ that are the signal power estimates in the H and V channels and $\hat{R}_{\rm hv}(0)$ that is the cross-correlation estimate (computed from time series as in [31, eq. (13)]).

Assuming scatterers with statistically isotropic properties, the mathematical expectations of second-order estimates are

$$\begin{aligned}\left\langle \hat{S}_c \right\rangle &= \left\langle |s_{cc}(k,m)|^2 \right\rangle \int_\Omega \left| F_{\rm tc}^{\rm co} F_{\rm rc}^{\rm co} \right|^2 d\Omega + \left\langle \Delta \hat{S}_c(k) \right\rangle \\ \left\langle \hat{R}_{\rm hv}(0) \right\rangle &= \left\langle s_{\rm hh}^*(k,m) s_{\rm vv}(k,m) \right\rangle \int_\Omega \left( F_{\rm th}^{\rm co} F_{\rm rh}^{\rm co} \right)^* F_{\rm tv}^{\rm co} F_{\rm rv}^{\rm co} d\Omega \\ &\quad + \left\langle \Delta \hat{R}_{\rm hv}(0) \right\rangle \end{aligned} \tag{11}$$

where

$$F_{\rm rc}^{\rm co} = \sum_{i=0}^{N_s-1} {\rm BFC}_c(i) C_c(i) S F_{\rm rc}^{\rm co}(i). \tag{12}$$

In (11), the terms with the symbol $\Delta$ are residuals as in (4) and describe the effects of cross-polar patterns researched in other works. Herein, we are interested in the impact of mismatches

between H and V copolar beam shapes and the effects of cross-polar patterns are ignored for simplicity and briefness.

The system effects on polarimetric estimates are analyzed in case of spherical weather scatterers where a well-calibrated radar should measure $Z_{DR}$ of ~0 dB, $|\rho_{hv}(0)|$ larger than 0.995 [28], and $\phi_{DP}$ of 0°. If H and V copolar patterns are perfectly matched in shape but differ in gain, the correction of the system-induced $\hat{Z}_{DR}$ bias can be conducted using the knowledge of beam peaks only. However, if there is a difference in shapes such that one beam is wider than the other, the volumes of scatterers encompassed by the two beams are not the same which results in measurement errors. In the case of patterns in Fig. 3, $\hat{Z}_{DR}$ bias due to shape mismatch is ~0.026 dB. To put this into perspective, it is recommended that the bias of $Z_{DR}$ estimates is kept within ±0.1 dB for intrinsic (i.e., true) $Z_{DR}$ between 0 and 1 dB and less than 0.1 $\times Z_{DR}$ for larger $Z_{DR}$ values [32], [33]. Hence, this bias may be significant when constructively added with other biases (e.g., cross-coupling effects and differences in gain). The expression for $\langle \hat{R}_{hv}(0) \rangle$ in (11) indicates that the beam mismatch has no effect on $\langle \hat{\phi}_{DP} \rangle$. However, if this expression is combined with $\langle \hat{S}_c \rangle$ to obtain the approximate expected value for $\langle |\hat{\rho}_{hv}(0)| \rangle$, it yields

$$\langle |\hat{\rho}_{hv}(0)| \rangle \approx \frac{\left| \left\langle s^*_{hh}(k,m) s_{vv}(k,m) \right\rangle \right|}{\sqrt{\left\langle |s_{hh}(k,m)|^2 \right\rangle \left\langle |s_{vv}(k,m)|^2 \right\rangle}} \times \frac{\left| \int_\Omega \left( F^{co}_{th} F^{co}_{rh} \right)^* F^{co}_{tv} F^{co}_{rv} d\Omega \right|}{\sqrt{\int_\Omega \left| F^{co}_{th} F^{co}_{rh} \right|^2 d\Omega \int_\Omega \left| F^{co}_{tv} F^{co}_{rv} \right|^2 d\Omega}}. \quad (13)$$

The expression (13) shows that the measured value of the copolar correlation coefficient is the product of intrinsic value imposed by scatterers (e.g., larger than 0.995 for most rainfall rates [28]) and the system-imposed correlation coefficient between the H and V copolar patterns. Hence, it is important that the latter value is as close to unity to maximize the accuracy of the copolar correlation coefficient estimation. For receive patterns shown in Fig. 3, this value is (since the transmit patterns are not measured)

$$\frac{\left| \int_\Omega \left( F^{co}_{rh} \right)^* F^{co}_{rv} d\Omega \right|}{\sqrt{\int_\Omega \left| F^{co}_{rh} \right|^2 d\Omega \int_\Omega \left| F^{co}_{rv} \right|^2 d\Omega}} = 0.992. \quad (14)$$

Clearly, the accuracy of the subarray phase and magnitude alignment prior to summation affects the quality and the matching of H and V receive beams. For this reason, the subarray magnitudes and phases are examined in Fig. 4, which indicates nonideal alignment. This in turn suggests that the system components prior to the test signal injection points affect the subarray alignment.

To improve the magnitude alignment, the average magnitude of a small area around the peaks (of the receive H and V patterns) is found (to minimize the effects of measurement fluctuations) for each subarray pattern. Then, BFC magnitudes are derived that scale the subarray magnitudes to approximately the same level. Next, subarray phases are equalized separately for each data point in the small area around the H and V beam peaks and the corresponding mean square error (MSE)

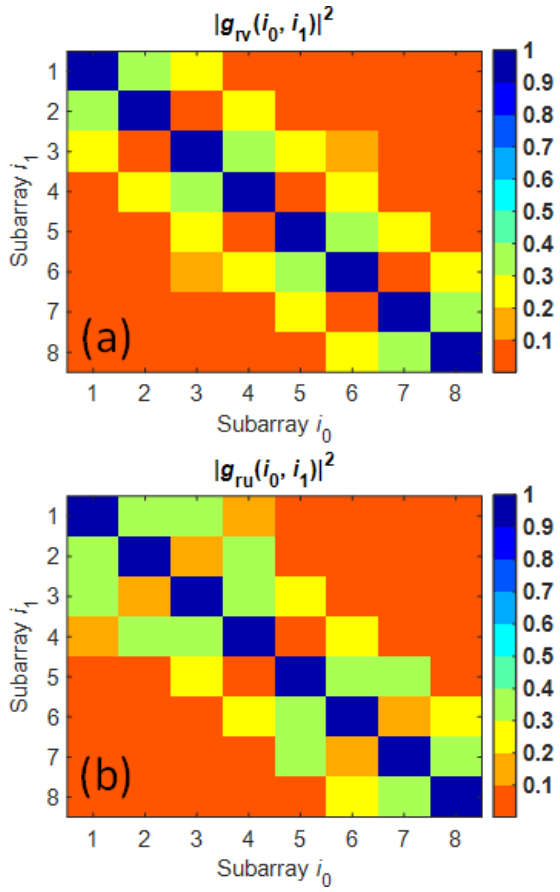


Fig. 7. $|g_{rc}(i_0, i_1)|^2$ values for (a) $v$- and (b) $u$-polarized subarrays.

between the resulting H and V patterns is computed for each. Out of all tested points, the equalization for the point that results in the smallest MSE is chosen. After magnitude and phase equalization, the improved alignment is presented in Fig. 5. Summation of data from orthogonally polarized channels results in the copolar receive beams with improved matching as shown in Fig. 6 where the value computed in (14) increases to 0.999. This demonstrates that, for this particular system, additional alignment that accounts for the effects of system components before the test signal injections improves the overall beam quality.

Another important aspect is the variance of the subarray correlation coefficient estimate that is [34]

$$\begin{aligned} &\mathrm{Var}\left[\arg\{\hat{\rho}_{sc}(i_0, i_1)\}\right] \\ &= \mathrm{Re}\left\{ \mathrm{Var}\left[|\hat{\rho}_{sc}(i_0, i_1)|^2\right] - \exp\left[-j2\arg\{g_c(i_0, i_1)\}\right] \right. \\ &\qquad \left. \times \mathrm{Var}\left[\hat{\rho}^2_{sc}(i_0, i_1)\right] \right\} \frac{1}{2|g_c(i_0, i_1)|^2} \end{aligned} \quad (15)$$

where

$$g_c(i_0, i_1) = \frac{C_c(i_0) C^*_c(i_1) \int_\Omega \left| F^{co}_{tc} \right|^2 S F^{co}_{rc}(i_0) S F^{co*}_{rc}(i_1) d\Omega}{\sqrt{\int_\Omega \left| F^{co}_{tc} S F^{co}_{rc}(i_0) \right|^2 d\Omega \times \int_\Omega \left| F^{co}_{tc} S F^{co}_{rc}(i_1) \right|^2 d\Omega}}. \quad (16)$$

The expression (15) shows that the variance of the system-imposed phase difference estimate between subarrays $i_0$ and $i_1$ is inversely proportional to $|g_c(i_0, i_1)|^2$. Note that the

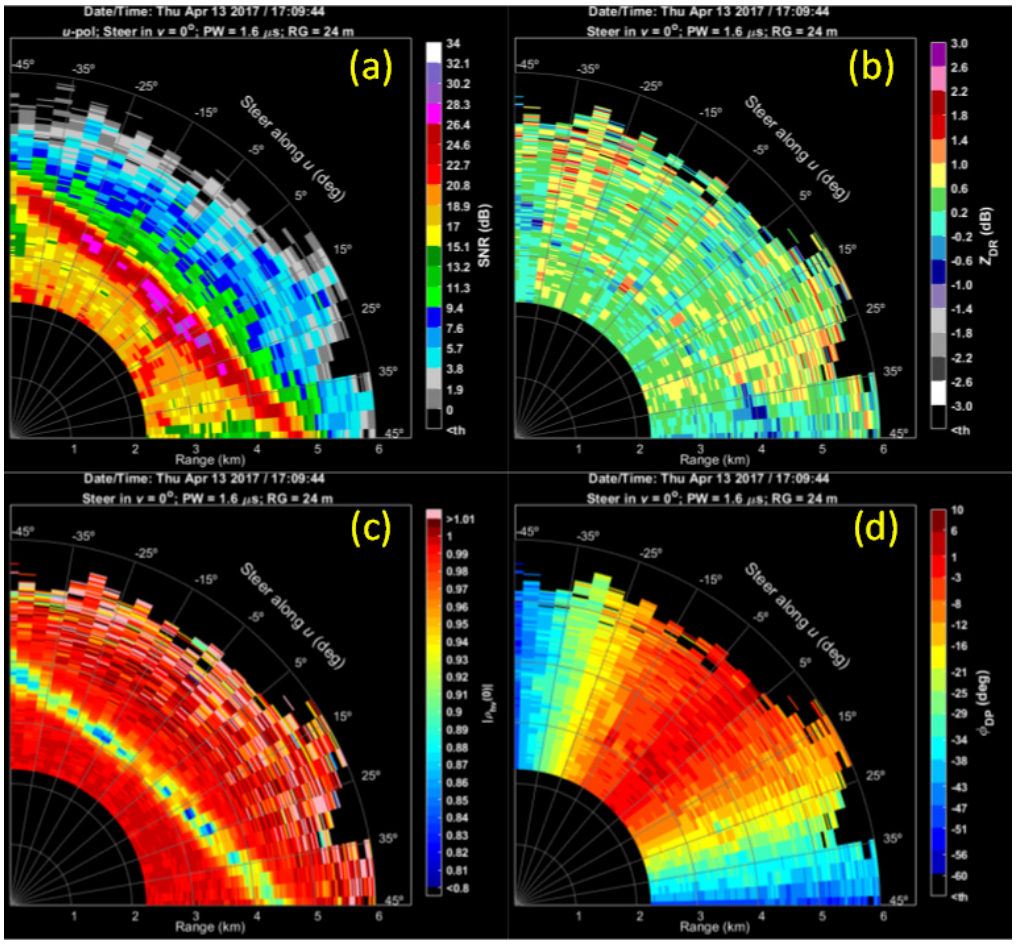


Fig. 8. Experimental data: (a) SNR, (b) differential reflectivity, (c) copolar correlation coefficient, and (d) differential phase field.

expression in (16) is the same as in (7), but the value of $\langle\hat{\rho}_{sc}(i_0, i_1)\rangle$ is only approximated in (7) and is, therefore, not used in (15). Because the transmit patterns are not measured and the value in (16) is dominated by the difference between receive subarray patterns [i.e., $\mathrm{SF}_{rc}^{co}(i_0)$ and $\mathrm{SF}_{rc}^{co}(i_1)$], values in (16) can be computed using only receive patterns as

$$|g_{rc}(i_0, i_1)|^2 = \frac{\left|\int_\Omega \mathrm{SF}_{rc}^{co}(i_0)\mathrm{SF}_{rc}^{co*}(i_1)d\Omega\right|^2}{\int_\Omega \left|\mathrm{SF}_{rc}^{co}(i_0)\right|^2 d\Omega \times \int_\Omega \left|\mathrm{SF}_{rc}^{co}(i_1)\right|^2 d\Omega}. \quad (17)$$

The values for $|g_{rc}(i_0, i_1)|^2$ for both polarizations are shown in Fig. 7 and can be used as a proxy for $|g_c(i_0, i_1)|^2$ (e.g., values in each column indicate $|g_c(i_0, i_1)|^2$ for $i_0$ and $i_1$ being the column and row numbers, respectively). These indicate that the subarrays 3–6 exhibit the higher average $|g_c(i_0, i_1)|$ values (along columns 3–6) than other subarrays. Consequently, using one of these subarrays as reference subarray $i_{ref}$ to estimate the subarray correlation coefficients (with respect to it) results in the overall lower estimate variances [as suggested by (15)].

### *B. Improved Alignment Using Weather Returns*

An experimental evaluation is conducted using a set of phase-coded data collected at vertical incidence in light-to-moderate rain (as previously indicated). During collection, the test signals were measured every ∼1.55 s and used to compute BFCs. The radar beam was steered electronically between −45° and 45° with respect to broadside and along $u$ principal axis (i.e., steering in $v = 0°$) with 3° step. At each steering position, data from 200 pulses were collected. The transmitted pulse width was 1.6 $\mu$s, and the sampling in range was 24 m. The pulses were transmitted at a rate of 1000 Hz. The radar operated at 2.87 GHz ($\lambda = 10.446$ cm). Due to the receiver protection limitations, the blind range was ∼2.3 km. At each beam position, the radial-based noise power estimation (RBNE) technique [35], [36] was applied to estimate the noise power and produce the signal-to-noise-ratio (SNR) field shown in Fig. 8(a). It shows that the majority of strong returns are from locations up to and including the melting layer (located at the height of ∼3 km and visible as the line of signals with SNR above ∼21 dB which stretches from −45° to 45°). The location of the melting layer is also observable via the characteristic drop in the copolar correlation coefficient in Fig. 8(c) [24], [30]. Note that the range given in Fig. 8 is not the actual height (except at $u = 0°$ when the beam is perpendicular to the ground) due to the variable beam angle with respect to the ground. Note that the melting layer appears as a straight line because the antenna was pointed at the sky. Also, an accurate estimation of noise powers was very important for the measurement of variables in Fig. 8 (especially the estimation of $|\rho_{hv}(0)|$ [36]) due to moderate SNRs (i.e., below ∼22 dB). The differential phase field is presented in Fig. 8(d). It indicates visible variation

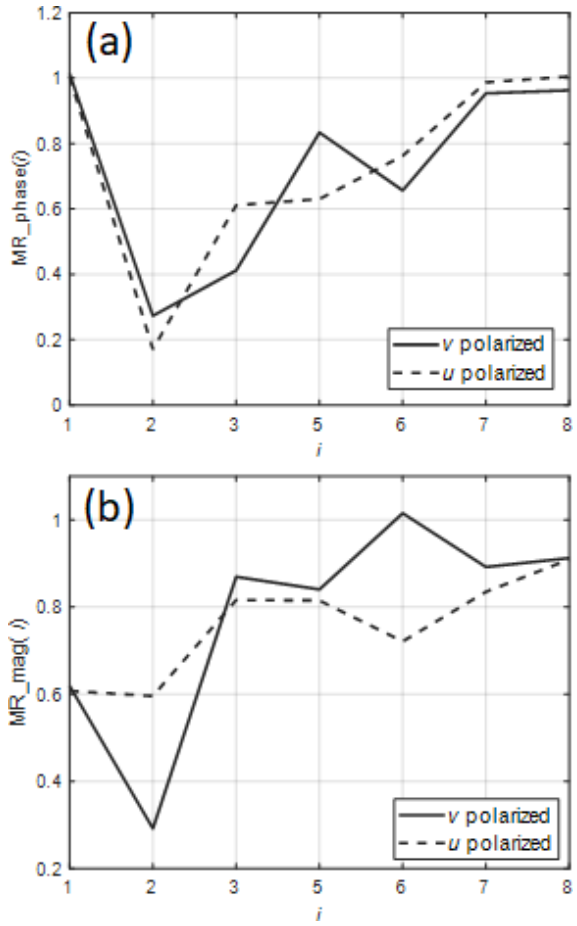


Fig. 9. Misalignment ratio for (a) phases and (b) magnitudes.

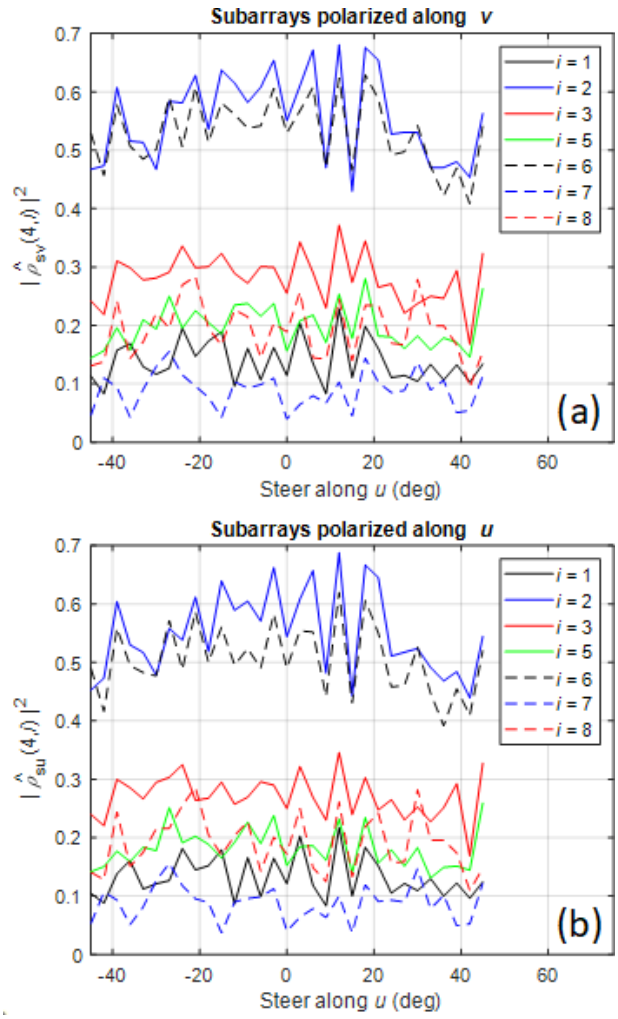


Fig. 10. Subarray correlation coefficients estimated from weather for subarrays polarized along (a) $v$ and (b) $u$.

with beamsteering position but no apparent change with range. This suggests that the system (and not the observed weather scatterers) causes the variations in the measured $\phi_{\mathrm{DP}}$.

The subarray phases and powers were estimated from the data and were used to update the existing BFCs [as specified in (10)] where subarray 4 was chosen as reference (i.e., $i_{\mathrm{ref}} = 4$). The following two quantities were computed to assess the reduction in the misalignment among subarrays. The first quantity is the phase misalignment ratio computed as

$$\mathrm{MR\_phase}(i) = \frac{\sum_{n=-15}^{15} \left|\arg\left\{\hat{\rho}_{sc}^{\mathrm{SAP}}(4,i,n\Delta u)\right\}\right|}{\sum_{n=-15}^{15} \left|\arg\{\hat{\rho}_{sc}(4,i,n\Delta u)\}\right|} \tag{18}$$

and the second is magnitude misalignment ratio obtained as

$$\mathrm{MR\_mag}(i) = \frac{\sum_{n=-15}^{15} \left|\widehat{\mathrm{SR}}_c^{\mathrm{SAP}}(4,i,n\Delta u)\right|}{\sum_{n=-15}^{15} \left|\widehat{\mathrm{SR}}_c(4,i,n\Delta u)\right|}. \tag{19}$$

The sums in the numerators of (18) and (19) are computed after the BFC update (note SAP in the superscript), while the denominators provide the values of the same sums before the BFC update. Note that the third argument is added to denote estimates across all beamsteering positions (i.e., $\Delta u = 3°$). The results for these quantities are shown in Fig. 9 and demonstrate a visible reduction in the misalignment factors after applying updated BFCs derived from weather measurements. For reference, the subarray correlation coefficients estimated from weather data are presented in Fig. 10. Trend wise, these agree well with measurements shown in Fig. 7.

To assess the effects of the weather derived BFCs on the polarimetric variable ensemble averages, all estimates are averaged in a range up to the height of the melting layer. Given that the radar is pointed upward, drops appear spherical to the radar, which makes the expected values of estimates uniform up to the melting layer. The results are demonstrated in Fig. 11.

The values for $\hat{Z}_{\mathrm{DR}}$ [Fig. 11(a)] exhibit a slight systematic increase in level after the SAP application. This is likely due to subarray magnitude equalization via SAP. The mean difference is 0.136 dB, while the maximum and minimum differences are 0.24 and 0.04 dB, respectively. In the case of $|\hat{\rho}_{\mathrm{hv}}(0)|$ [Fig. 11(b)], the application of SAP produces a visible increase in the value of estimates, which indicates an improved matching between the H and V copolar beam shapes. The mean difference is 0.0027, while the maximum and minimum differences are 0.005 and 0.0008, respectively. Finally, the $\hat{\phi}_{\mathrm{DP}}$ results in Fig. 11(c) show no visible differences before and after the SAP application. This corroborates the conclusion drawn from (11) that the beam mismatch has little to no effect on $\hat{\phi}_{\mathrm{DP}}$ expected values. Next, the effect of SAP application

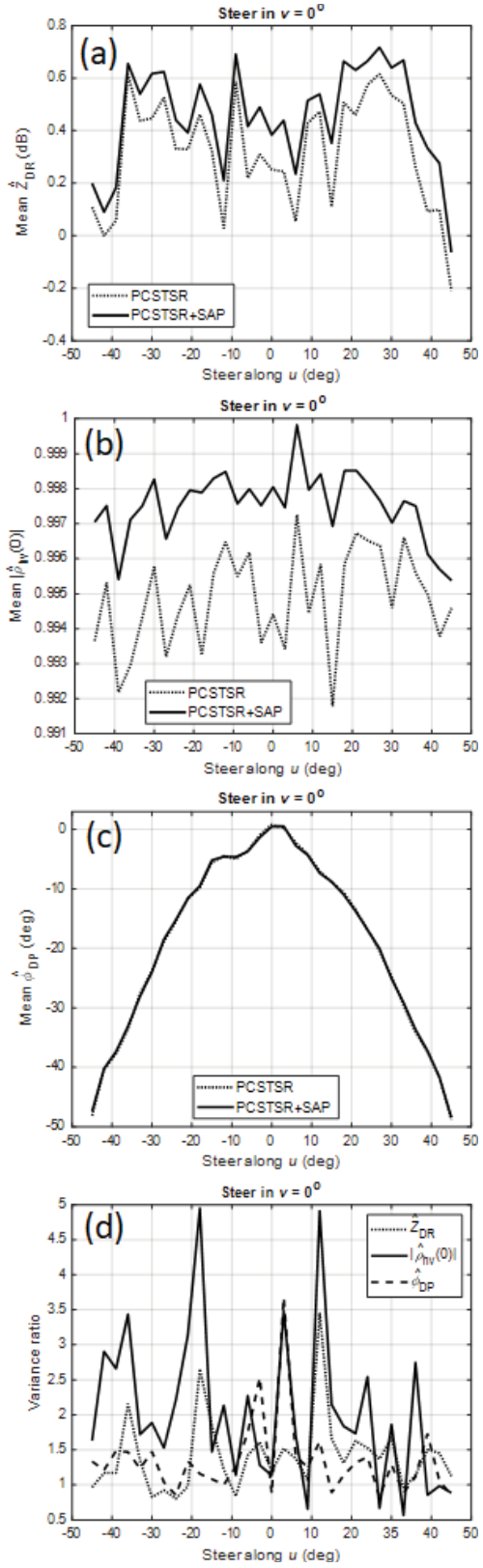


Fig. 11. Range-averaged values of polarimetric variable estimates before and after SAP application for (a) $Z_{DR}$, (b) $|\rho_{hv}(0)|$, and (c) $\phi_{DP}$. (d) Ratio of variances before and after SAP application.

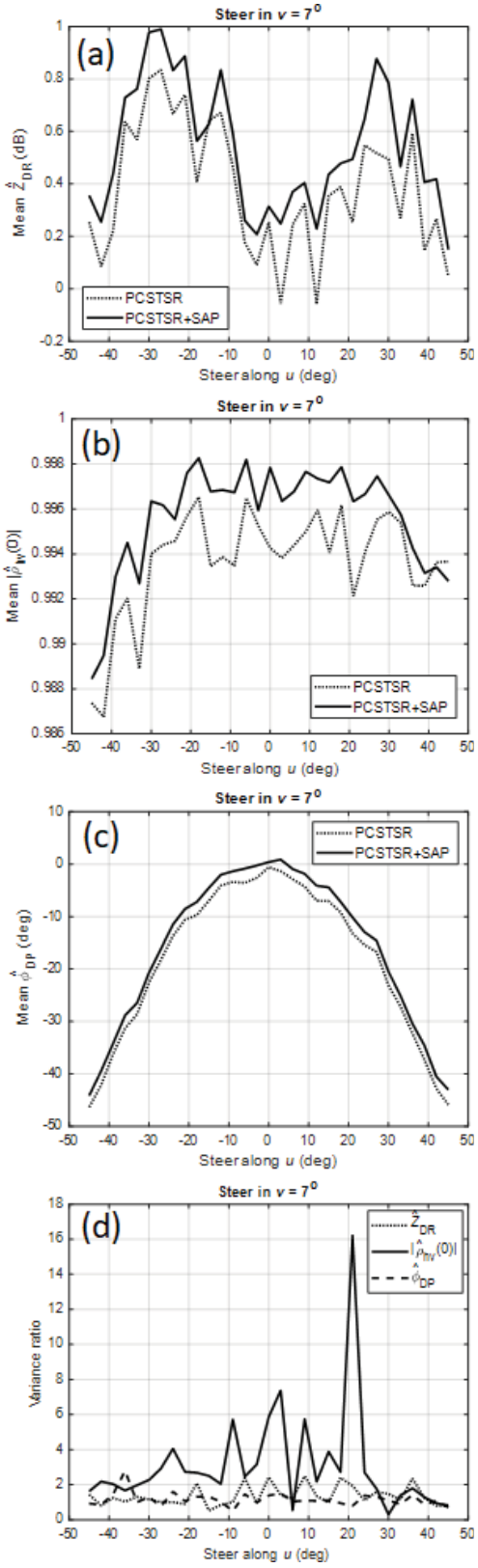


Fig. 12. Range-averaged values of polarimetric variable estimates before and after SAP application for (a) $Z_{DR}$, (b) $|\rho_{hv}(0)|$, and (c) $\phi_{DP}$. (d) Ratio of variances before and after SAP application.

on the variance of polarimetric estimates is examined. For this purpose, the variance at each beam position is computed before and after SAP application for each polarimetric variable.

The ratios of variances (without SAP versus with SAP) are shown in Fig. 11(d). The mean ratios are 1.4, 2, and 1.34 for the variances of $\hat{Z}_{DR}$, $|\hat{\rho}_{hv}(0)|$, and $\hat{\phi}_{DP}$, respectively.

These values imply that the application of SAP results in the variance reduction on the average. This effect may be intuitively explained by noting that the number of nonidentically weighted scatterers (i.e., scatterers weighted significantly by the H copolar main beam but suppressed by V and vice versa) is directly proportional to the degree of H and V copolar beam shape mismatch and vice versa. Because these nonidentical scatterers contribute to the increase in the variance of polarimetric variable estimates, reducing their number results in the variance reduction.

For completeness, another data set collected at vertical incidence was processed and the results are shown in Fig. 12. The only difference from the previous set is that the steering in $\upsilon$ was set to 7°. The mean differences between estimates of $\hat{Z}_{\mathrm{DR}}$, $|\hat{\rho}_{\mathrm{hv}}(0)|$, and $\hat{\phi}_{\mathrm{DP}}$ with and without SAP are 0.16 dB, 0.002, and 2.3°, respectively. The mean ratios of variances before and after SAP application are 1.37, 3.09, and 1.17 for $\hat{Z}_{\mathrm{DR}}$, $|\hat{\rho}_{\mathrm{hv}}(0)|$, and $\hat{\phi}_{\mathrm{DP}}$, respectively. Trend wise, these results agree with those from the previous data set and corroborate the previously stated findings. More examples can be found in [37].

## V. Summary and Conclusion

In this article, a novel method to measure the phase and magnitude differences among receive subarrays using returns from hydrometeors is presented. Such measurements can be used to update the existing or compute the new beamforming coefficients (i.e., the set of complex numbers used to weigh the output of each subarray to achieve the phase and magnitude alignment). This has the potential to increase the accuracy of beamforming coefficients and improve the quality of the horizontally and vertically polarized copolar antenna patterns as well as the matching between them. This, in turn, results in the more precise and accurate estimates of differential reflectivity and copolar correlation coefficient.

The method is evaluated using a mobile dual-polarized PAR system with eight subarrays referred to as Ten Panel Demonstrator (TPD). To measure the phase differences among receivers, test signals are injected at the TPD downconverter inputs. The test signal measurements are used to create the set of unit modulus complex numbers that are used to weight data from individual subarrays (i.e., beamforming coefficients) prior to summation. The application of these weights removes the channel-to-channel phase differences incurred by the downconverters and the subsequent circuitry. Thus, so obtained beamforming coefficients do not correct for phase differences introduced by the hardware prior to the test signal injection point nor any magnitude differences among subarrays.

Analysis of data collected using a horn antenna (used to transmit toward TPD) indicated the mismatch in shape between the horizontal and vertical receive patterns. Concurrently, data from individual subarrays revealed the potential for improvement of alignment among the subarray phases and magnitudes. Consequently, it is demonstrated that the matching of horizontal and vertical receive patterns improves after the phase and magnitude equalization. Further, it is shown that the copolar correlation coefficient measured by the polarimetric radar is the product of the weather and system-dependent terms. Thus, it is crucial that the latter term is as close to unity as possible, to facilitate accurate measurement of weather properties. In this regard, it is demonstrated that the system-dependent term increases in value and further approaches unity after refining the phase and magnitude alignment. This serves as an experimental verification of the benefits that the proposed method can provide (as it delivers the relative phase and magnitude measurements of the full subarray receive paths).

Subsequent analysis was conducted on weather data collected at vertical incidence whereby the proposed method was experimentally evaluated. It is shown that the weather data can be used to estimate the relative differences among subarray phases and magnitudes. Further, these estimates were used to modify the existing beamforming coefficients. The application of modified coefficients resulted in the systematic increase in the copolar correlation coefficient estimates. Because this measurement is the product of the weather and system-dependent terms, this is a strong indication of the enhanced shape matching between horizontal and vertical two-way copolar patterns (resulting from the application of the modified beamforming coefficients). Evaluation of polarimetric variable estimate variances also revealed an average reduction after improvement of beam shape matching. Because the copolar correlation coefficient is most sensitive to the shape mismatch between orthogonally polarized main beams, this product exhibits the largest variance reduction.

Herein, the proposed method is evaluated using the system with infrastructure for creating beamforming coefficients (i.e., test signals). Nonetheless, the method can be readily applied to systems that do not furnish such infrastructure. Further, the experimental evaluation of the method is conducted on data collected at vertical incidence. Nonetheless, the method should be readily applicable to data sets collected with the antenna perpendicular or tilted relative to the ground.

## Acknowledgment

The author would like to thank Dr. Duš an S. Zrnić, Dr. Feng Nai, and David Schvartzman who reviewed this article and provided valuable comments that enhanced it. He would also like to thank anonymous reviewers whose comments improved the text. The statements, findings, conclusions, and recommendations are those of the author(s) and do not necessarily reflect the views of NOAA or the U.S. Department of Commerce.

## References

[1] D. S. Zrnić *et al.*, "Agile-beam phased array radar for weather observations," *Bull. Amer. Meteorol. Soc.*, vol. 88, no. 11, pp. 1753–1766, Nov. 2007.

[2] P. L. Heinselman and S. M. Torres, "High-temporal-resolution capabilities of the national weather radar testbed phased-array radar," *J. Appl. Meteorol. Climatol.*, vol. 50, no. 3, pp. 579–593, Mar. 2011, doi: 10.1175/2010jamc2588.1.

[3] J. E. Stailey and K. D. Hondl, "Multifunction phased array radar for aircraft and weather surveillance," *Proc. IEEE*, vol. 104, no. 3, pp. 649–659, Mar. 2016. [Online]. Available: http://ieeexplore.ieee.org/document/7393756/

[4] S. M. Torres *et al.*, "Adaptive-weather-surveillance and multifunction capabilities of the national weather radar testbed phased array radar," *Proc. IEEE*, vol. 104, no. 3, pp. 660–672, Mar. 2016, doi: 10.1109/JPROC.2015.2484288.

[5] D. S. Zrnić, V. M. Melnikov, and R. J. Doviak, "Issues and challenges for polarimetric measurement of weather with an agile beam phased array radar," NOAA/NSSL, Norman, OK, USA, Tech. Rep., 2012, p. 119. [Online]. Available: https://www.nssl.noaa.gov/publications/mpar_reports/

[6] M. C. Leifer, V. Chandrasekar, and E. Perl, "Dual polarized array approaches for MPAR air traffic and weather radar applications," in *Proc. IEEE Int. Symp. Phased Array Syst. Technol.*, Waltham, MA, USA, Oct. 2013, pp. 485–489. [Online]. Available: https://ieeexplore.ieee.org/document/6731876

[7] M. E. Weber, "Meteorological phased array radar research at NOAA's National Severe Storms Laboratory," in *Proc. IEEE Int. Conf. Microw., Antennas, Commun. Electron. Syst. (COMCAS)*, Tel-Aviv, Israel, Nov. 2019, pp. 1–6. [Online]. Available: https://ieeexplore.ieee.org/document/8958067

[8] D. S. Zrnić and A. V. Ryzhkov, "Polarimetry for weather surveillance radars," *Bull. Amer. Meteorol. Soc.*, vol. 80, no. 3, pp. 389–406, Mar. 1999.

[9] R. J. Doviak and D. S. Zrnić, *Doppler Radar and Weather Observations*. San Diego, CA, USA: Academic, 1993, p. 562.

[10] V. Bringi and V. Chandrasekar, *Polarimetric Doppler Weather Radar*. Cambridge, U.K.: Cambridge Univ. Press, 2001, p. 636.

[11] D. S. Zrnić, V. M. Melnikov, and J. K. Carter, "Calibrating differential reflectivity on the WSR-88D," *J. Atmos. Ocean. Technol.*, vol. 23, no. 7, pp. 944–951, Jul. 2006, doi: 10.1175/jtech1893.1.

[12] J. C. Hubbert, "Differential reflectivity calibration and antenna temperature," *J. Atmos. Ocean. Technol.*, vol. 34, no. 9, pp. 1885–1906, Sep. 2017, doi: 10.1175/JTECH-D-16-0218.1.

[13] I. R. Ivić, "Options for polarimetrie variable measurements on the MPAR advanced technology demonstrator," in *Proc. IEEE Radar Conf. (RadarConf)*, Oklahoma City, OK, USA, Apr. 2018, pp. 129–134, doi: 10.1109/RADAR.2018.8378544.

[14] C. Fulton, J. Salazar, D. Zrnić, D. Mirković, I. R. Ivić, and D. Doviak, "Polarimetrie phased array calibration for large-scale multimission radar applications," in *Proc. IEEE Radar Conf. (RadarConf)*, Oklahoma City, OK, USA, Apr. 2018, pp. 1272–1277, doi: 10.1109/RADAR.2018.8378746.

[15] D. S. Zrnić, R. J. Doviak, V. M. Melnikov, and I. R. Ivić, "Signal design to suppress coupling in the polarimetric phased array radar," *J. Atmos. Ocean. Technol.*, vol. 31, no. 5, pp. 1063–1077, May 2014, doi: 10.1175/jtech-d-13-00037.1.

[16] I. R. Ivić and R. J. Doviak, "Evaluation of phase coding to mitigate differential reflectivity bias in polarimetric PAR," *IEEE Trans. Geosci. Remote Sens.*, vol. 54, no. 1, pp. 431–451, Jan. 2016, doi: 10.1109/TGRS.2015.2459047.

[17] I. R. Ivić, "An experimental evaluation of phase coding to mitigate the cross-coupling biases in PPAR," in *Proc. 38th Int. Conf. Radar Meteorol.*, Chicago, IL, USA, Aug./Sep. 2017, p. 1. [Online]. Available: https://www.researchgate.net/publication/319914859_An_Experimental_Evaluation_of_Phase_Coding_to_Mitigate_the_Cross-Coupling_Biases_in_PPAR

[18] I. R. Ivić *et al.*, "An overview of weather calibration for the advanced technology demonstrator," in *Proc. IEEE Int. Symp. Phased Array Syst. Technol.*, Waltham, MA, USA, Oct. 2019, pp. 1–7. [Online]. Available: https://www.researchgate.net/publication/338019168_An_Overview_of_Weather_Calibration_on_the_Advanced_Technology_Demonstrator

[19] I. R. Ivić and D. Schvartzman, "A first look at the ATD data corrections," in *Proc. 39th Int. Conf. Radar Meteorol.*, Nara, Japan, Sep. 2019, pp. 2–6. [Online]. Available: https://www.researchgate.net/publication/336409584_A_first_look_at_the_ATD_data_corrections

[20] J. S. Herd, S. M. Duffy, and H. Steyskal, "Design considerations and results for an overlapped subarray radar antenna," in *Proc. IEEE Aerosp. Conf.*, Mar. 2005, pp. 1087–1092, doi: 10.1109/AERO.2005.1559399.

[21] M. Galletti and D. S. Zrnić, "Bias in copolar correlation coefficient caused by antenna radiation patterns," *IEEE Trans. Geosci. Remote Sens.*, vol. 49, no. 6, pp. 2274–2280, Jun. 2011, doi: 10.1109/TGRS.2010.2095019.

[22] S. Chaudhary and A. Samant, "Characterization and calibration techniques for multi-channel phase-coherent systems," *IEEE Instrum. Meas. Mag.*, vol. 19, no. 4, pp. 44–50, Aug. 2016.

[23] C. Fulton and W. Chappell, "Calibration techniques for digital phased arrays," in *Proc. IEEE Int. Conf. Microw., Commun., Antennas Electron. Syst. (COMCAS)*, Nov. 2009, pp. 1–10.

[24] D. Conway *et al.*, "On the development of a tileable LRU for the nextgen surveillance and weather radar capability program," in *Proc. IEEE Int. Symp. Phased Array Syst. Technol.*, Oct. 2013, pp. 490–493.

[25] I. R. Ivić and A. Byrd, "A first look at the MPAR dual-polarization phased-array-radar mobile demonstrator," in *Proc. 37th Conf. Radar Meteorol.*, Norman, OK, USA, Sep. 2015, p. 1, doi: 10.13140/RG.2.2.33278.79683.

[26] S. V. Nghiem, S. H. Yueh, R. Kwok, and F. K. Li, "Symmetry properties in polarimetric remote sensing," *Radio Sci.*, vol. 27, no. 5, pp. 693–711, Sep./Oct. 1992.

[27] T. Oguchi, "Electromagnetic wave propagation and scattering in rain and other hydrometeors," *Proc. IEEE*, vol. 71, no. 9, pp. 1029–1078, Sep. 1983.

[28] M. Sachidananda and D. S. Zrnić, "ZDR measurement considerations for a fast scan capability radar," *Radio Sci.*, vol. 20, no. 4, pp. 907–922, Jul. 1985.

[29] A. V. Ryzhkov and D. S. Zrnić, "Depolarization in ice crystals and its effect on radar polarimetric measurements," *J. Atmos. Ocean. Technol.*, vol. 24, no. 7, pp. 1256–1267, Jul. 2007, doi: 10.1175/JTECH2034.1.

[30] A. Illingworth and R. J. Thompson, "Radar bright band correction using the linear depolarisation ratio," in *Proc. 8th Int. Symp. Weather Radar Hydrol.*, Exeter, U.K., Apr. 2011, p. 5. [Online]. Available: http://www.met.reading.ac.uk/radar/publications/LDR.pdf

[31] I. R. Ivić, "Phase code to mitigate the copolar correlation coefficient bias in PPAR weather radar," *IEEE Trans. Geosci. Remote Sens.*, vol. 55, no. 4, pp. 2144–2166, Apr. 2017, doi: 10.1109/TGRS.2016.2637720.

[32] D. Zrnić, R. Doviak, G. Zhang, and A. Ryzhkov, "Bias in differential reflectivity due to cross coupling through the radiation patterns of polarimetric weather radars," *J. Atmos. Ocean. Technol.*, vol. 27, no. 10, pp. 1624–1637, Oct. 2010, doi: 10.1175/2010jtecha1350.1.

[33] Y. Wang and V. Chandrasekar, "Polarization isolation requirements for linear dual-polarization weather radar in simultaneous transmission mode of operation," *IEEE Trans. Geosci. Remote Sens.*, vol. 44, no. 8, pp. 2019–2028, Aug. 2006, doi: 10.1109/TGRS.2006.872138.

[34] F. C. Benham, H. L. Groginsky, A. S. Soltes, and G. Works, "Pulse pair estimation of Doppler spectrum parameters," Raytheon Company, Waltham, MA, USA, Tech. Rep., 1972, p. 157.

[35] I. R. Ivić, C. Curtis, and S. M. Torres, "Radial-based noise power estimation for weather radars," *J. Atmos. Ocean. Technol.*, vol. 30, no. 12, pp. 2737–2753, Dec. 2013, doi: 10.1175/jtech-d-13-00008.1.

[36] I. R. Ivić, "On the use of a radial-based noise power estimation technique to improve estimates of the correlation coefficient on dual-polarization weather radars," *J. Atmos. Ocean. Technol.*, vol. 31, no. 9, pp. 1867–1880, Sep. 2014, doi: 10.1175/JTECH-D-14-00052.1.

[37] I. R. Ivić, "An approach to align subarray channels in PPAR using weather returns," in *Proc. 38th Int. Conf. Radar Meteorol.*, Chicago, IL, USA, Aug./Sep. 2017, pp. 1–2. [Online]. Available: https://www.researchgate.net/publication/319914863_An_Approach_to_Align_Subarray_Channels_in_PPAR_Using_Weather_Returns

**Igor R. Ivić** received the B.S. degree in electrical engineering from the University of Novi Sad, Novi Sad, Serbia, in 1996, and the M.Sc. and Ph.D. degrees in electrical engineering from the University of Oklahoma, Norman, OK, USA, in 2001 and 2008, respectively.

From 1996 to 1997, he was a Research Associate at the School of Computer Science, Faculty of Technical Sciences, Novi Sad. In 1997, he joined the National Severe Storms Laboratory (NSSL) through the Cooperative Institute for Mesoscale Meteorological Studies, University of Oklahoma. From 1997 to 2009, he was a Research Associate, and since 2009, he has been a Research Scientist at NSSL. His research interests include weather radar signal processing, advancements of polarimetric measurements, development of algorithms for the national network of weather radars (WSR-88D), and applications of agile beam phased-array radar for weather observations.

Dr. Ivić received the Department of Commerce Silver Medal as a member of Stormscale Research and Applications Division at the National Severe Storms Laboratory for making significant enhancements to the NEXRAD systems and the Outstanding Scientific Paper Award from the Office of Oceanic and Atmospheric Research, U.S. Department of Commerce in 2005.